The Bioscan AN INTERNATIONAL QUARTERLY JOURNAL OF LIFE SCIENCES 21(1) 1626-1644, 2026 www.thebioscan.com

A Green Emitting Organic Non-linear Optical Crystal (E)-4-Bromo-2-(((2-(2-hydroxyethoxy)ethyl)imino)methyl)phenol: Crystal Structure, Spectroscopic studies, Anticancer Activity

Priyanka. J[1], Ida Malarselvi. R[1*], Vinitha. G[2], Ramachandra Raja. C[1] and Priscilla. R[3]

[1] Research Centre, Department of Physics, D. G. Government Arts College (W), (Affiliated Bharathidasan University), Mayiladuthurai 609 001, Tamil Nadu, India.
[2] Division Physics, School of Advanced-Science, Vellore Institute of Technology, Chennai 600 127, Tamil Nadu, India.
[3] Postgraduate Department of Physics, A.D.M. College (W) (Autonomous), (Affiliated Bharathidasan University), Nagapattinam 611 001, Tamil Nadu, India.
Corresponding author's mail: idamalarselvi@gmail.com

DOI: https://doi.org/10.63001/tbs.2026.v21.i01.pp1626-1644

Keywords:
Crystal Structure,
Mid-IR,
Z-Scan

Received on: 14-01-2026

Revised on: 21-02-2026

Published on:09-03-2026

Abstract

(E)-4-Bromo-2(((2-(2-hydroxyethoxy)ethyl)imino)methyl)phenol (E-4B2HMP), a unique series of solid crystal, with a laser-induced damage threshold (LIDT) and a notable non-linear optical coefficient. The frequency conversion of mid-infrared lasers has excellent application opportunities for it. Using powder x-ray diffraction data and NMR guidance, a direct structural determination was carried out. The monoclinic P_{21} solved and improved the non-centrosymmetric structure. It is the first crystal in the family for non-linear frequency conversion that could be proved to have the highest nonlinearity and figure of merit for nonlinear optical applications in the mid-infrared. Here, we highlight the evolution of nonlinear optical processes, their use in bioimaging, and the most recent advancements in this field. The presence of a self-defocusing feature related to positive nonlinear refraction was established by the closed aperture Z-scan curves.

Introduction:

In recent years, mid-IR laser sources have attracted increasing attention due to their potential applications [1]. Imines are the compound that forms by the condensation reaction of the amine, a class of a well-known group of materials called Schiff base [2]. The development of highly efficient nonlinear optical crystals for extremely important for both laser spectroscopy and laser processing. Sufficiently large nonlinear areas, a low laser damage threshold power, and ease of growing with enormous dimensions are requirements for superior grade NLO organic crystals [3]. E-4B2HMP is a class of compounds that has a significant impact on the pharmaceutical industry. Recently, various techniques for producing non-centrosymmetric crystals have been developed [4].

Strong hydrogen bond interactions are known to be crucial for the composition of biological systems, molecular crystal structures, and crystal structures. Hydrogen bonding is

recognized as the most powerful force to organize molecules in the solid state and its employment is now emerging as an important design strategy [5]. Organic materials have the fundamental benefit of being able to modify their structure to obtain the necessary NLO characteristics. Organic NLO materials exhibit nonlinearity due to the delocalized π-electron that connects the donor and acceptor groups, hence elevating the necessary asymmetric polarizability. These compounds must crystallize in a non-centrosymmetric class for the application of quadratic nonlinear optical effects [6]. The organic NLO crystal's basic structure depends on the π bond interaction system. The orbital de-localization of the electronic-charge distribution must overlap in order to attain a high-mobility of electron density. Asymmetric electronic sharing in either or both excited states and ground states can be enhanced at either or both ends of the π-bond interaction system functionalized with appropriate electron donor and acceptor assemblies; these elements lead to enhanced optical nonlinearity. Due to the variety of organic NLO crystals, a great deal of study was conducted on the organic crystal. They discovered that an aromatic group compound with non-localized π-electron structures and a significant dipole moment was generated to advance the NLO susceptibilities higher than the inorganic materials. [7].

5-Bromo-2-hydroxybenzaldehyde and 2-(2-aminoethoxy) ethanol are interesting molecules for non-linear optical (NLO) applications as they contain a proton donor, -CHO group, and a proton acceptor, -NH2 group, which assures crystalline non-centrosymmetric. Although there were certain difficulties in determining the structure, these could be overcome by adding information from NMR data to the powder XRD analysis and using DASH 4.0.0 software to solve the problems. Powder X-ray diffraction and NMR spectroscopy are both used for crystalline materials [8]. Here, we discuss the synthesis, growth, and characterization of new organic E-4B2HMP crystal from the (E)-4-Bromo-2-(((2-(2-hydroxyethoxy)ethyl)imino)methyl)phenol family. The crystal structure is determined by the powder X-ray diffraction method using DASH 4.0.0 software. The structure of the compound has been confirmed by Nuclear Magnetic Resonance spectroscopy (NMR). Fourier Transform Infrared (FT-IR) has been recorded to analyze the functional group in the molecular structure of synthesized E-4B2HMP compound, and vibration analysis was studied. Fourier Transform Raman (FT-RAMAN), UV-vis spectroscopy, photoluminescence (PL), and laser damage threshold (LDT) characterization have been performed. We study systematically the nonlinear-absorption and nonlinear-refraction properties of E-4B2HMP crystal by Z-scan Analysis. The investigation of the potential of E-4B2HMP single crystal as NLO material and its applications would be made easier by this collaborative study with the aforementioned crucial criteria.

2. Experimental Section

2.1. Synthesis and Crystal Growth

Every substance was used exactly as it was purchased and was of the grade of an analytical reagent. The title compound was synthesized by reacting 5-Bromo-2-hydroxybenzaldehyde and 2-(2-aminoethoxy)ethanol in acetic acid 4:3 stoichiometric ratio. Crystal of (E)-4-Bromo-2(((2-hydroxyethoxy)ethyl)imino)methyl)phenol (E-4B2HMP) were harvested by slow solvent evaporation at room temperature in 10 days. The grown E-4B2HMP single crystal is shown in Figure 1. The reaction scheme is shown in Figure 2.

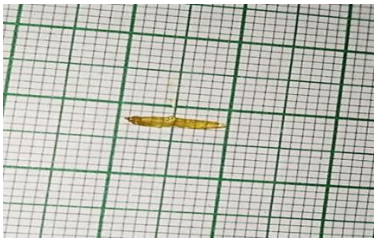

Figure 1. Grown crystal of E-4B2HMP

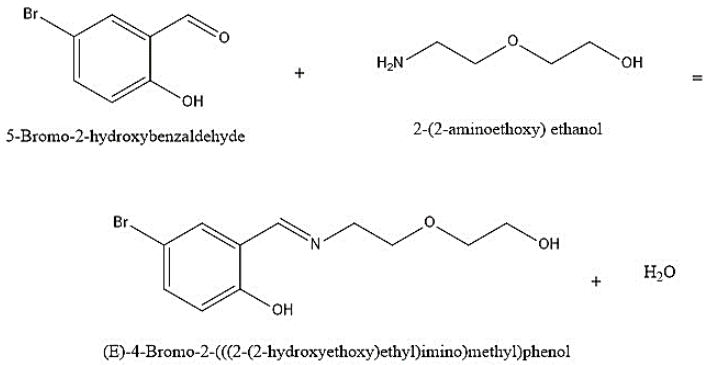

Figure 2. E-4B2HMP crystal's reaction scheme

3. Result and Discussion

3.1. Single crystal and Powder X-ray Diffraction Analyses

A Bruker Kappa APEXII diffractometer was used to acquire SCXRD data for a single crystal of E-4B2HMP using Cu(Kα) radiation in order to determine just the unit cell characteristics. The unit cell characteristics for the grown E-4B2HMP crystal have been determined by single crystal X-ray diffraction analysis. The E-4B2HMP crystal structure is a component of the non-centrosymmetric space group P_{21} monoclinic crystal system. The obtained lattice parameters are presented in Table 1.

An X'Pert Pro-PAnalytic was used to record PXRD utilizing Cu Kα radiation (λ= 1.5406 Å) at 40 kV and 30 mA power. The diffraction pattern of X-rays was recorded within the 2θ range of 10˚ to 80˚. The generated crystals were analysed using powder X-ray diffraction after being finely pulverized. The X-ray powder pattern is shown in Figure 3. Thus, the XRD analysis confirms the good crystallinity nature and purity of the title compound. Comparing the powder data to the single-crystal data, the lattice parameters are even more precise. When doing a thorough Structure determination from powder data (SDPD), mistakes about the space group, atom assignment, molecular composition, or hydrogen bond network are nearly as uncommon as they are in conventional single-crystal investigations [9].

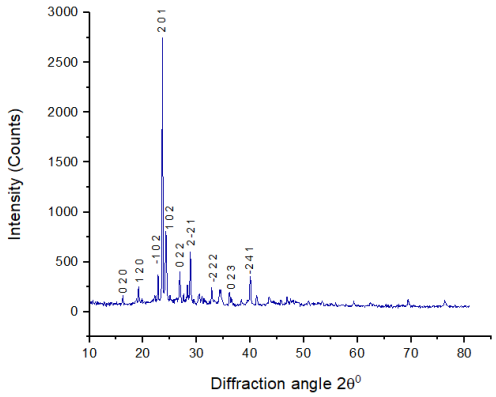

Figure 3 X-ray powder diffraction pattern of E-4B2HMP used for the structure determination

Table 1. Crystallographic data of E-4B2HMP

Parameter	Single Crystal XRD
a	4.28 Å
b	6.03 Å
c	15.66 Å
α	90˚
β	93.05˚
γ	90˚
System	Monoclinic
Lattice, space group	P

3.2. Structure Determination

Direct structural determination from powder-XRD data while considering NMR data [8]. DASH is a user-friendly computer program with a graphical user interface (GUI) that was developed specifically to identify crystal structures using X-ray powder diffraction data. For molecular structures, it is ideal. We used the Gaussian 16W, revision c.01, software, and the input module optimized by the keywords "opt hf/3-21g geom=connectivity" in DASH 4.0.0 to identify the crystal structure [10]. H_{27}-O_{10}…N_8 intramolecular hydrogen bonds are found in the structure (dashed blue lines). The best powder pattern was used for the indexing. The indexing was performed with DICVOL91 as it is implemented in the DASH software. The default settings were used for the remaining parameters that control the simulated annealing. There were no restrictions made on the flexible torsions. The number of simulated annealing runs was set to 50. The background fitting, Pawley refinement, and simulated annealing were used as implemented in the DASH software [9]. E-4B2HMP crystallizes in the Monoclinic space group P_{21}. Crystallographic data are given in Table 2. The molecule exhibits a quite elongated conformation in Figure 4.

Table 2 Crystallographic data of E-4B2HMP

Chemical Formula	$C_{11}H_{14}BrNO_3$
Molecular Weight	288.14
Crystal System	Monoclinic
a/ Å	8.79380
b/ Å	10.87710
c/ Å	8.38410
α/°	90
β/°	94.5110
γ/°	90
Unit Cell Volume/A^3	799.5
Space group	**P_{21}**
Z	2
Dx, g cm^{-3}	1.197
Temperature / K	308
2Θ range for data collection (˚)	10.0-80.0
Radiation, λ/ Å	Cu-Kα, 1.5406

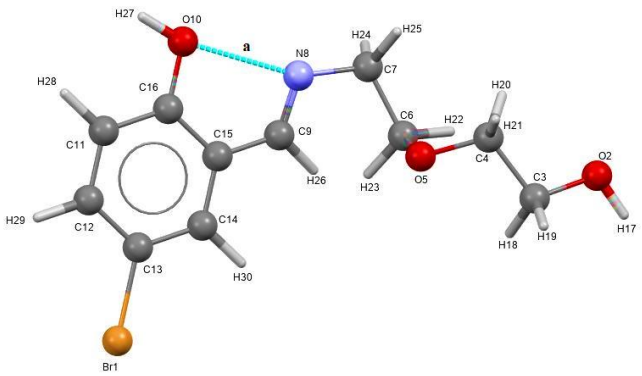

Figure 4 Molecular Structure of E-4B2HMP

3.3 ^{13}C and ^{1}H NMR analysis

NMR investigations examined the E-4B2HMP compound's molecular structure. After the sample was dissolved in DMSO, the ^{1}H and ^{13}C NMR spectra of the developed E-4B2HMP crystals were recorded. Table 3 compares the NMR spectra of 2-(2-aminoethoxy) ethanol and 5-Bromo-2-hydroxybenzaldehyde, which were gathered from the AIST: spectral database (https://sdbs.db.aist.go.jp)

A Bruker AMX NMR Spectrometer (300 MHz) was used to record the ^{13}C NMR profile of the E-4B2HMP molecule. Figure 5 shows the spectrum with the solvent being dimethyl sulfoxide (DMSO) and the internal reference being room temperature tetramethyl silane (TMS). The DMSO solvent's peak is seen at 39.935 ppm. The chemical shift observed at 138.892 ppm, 130.923 ppm, 124.443 ppm, 120.326 ppm, and 111.176 ppm was attributed to the carbon atom of the aromatic ring. At 192.70 ppm, the CHO resonance signal was detected. The downfield shift of the peak from

192.70 ppm to 190.118 ppm indicates that water molecules were eliminated during the chemical E-4B2HMP's manufacturing technique. This signal was identified at 111.176 ppm because of the location of the carbon atom in the Br halides group. The triplet that was seen at 39.433 ppm, 39.602 ppm, and 39.768 ppm is caused by the carbon atom that is present in the (phenol)OH group of 2-(2-aminoethoxy)ethanol.

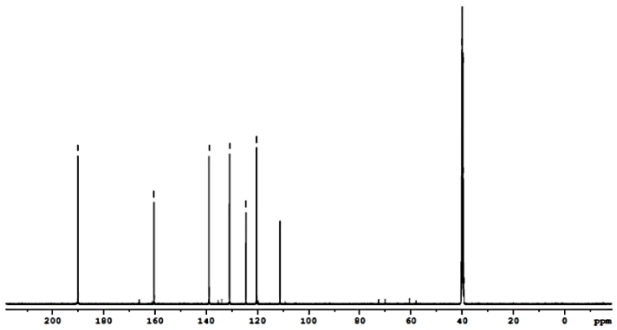

Figure 5. ^{13}C NMR Spectrum of E-4B2HMP compound

The Bruker AMX NMR Spectrometer (300 MHz) was used to record the ^{1}H NMR profile of the E-4B2HMP molecule. Tetramethyl silane is used as an reference at room temperature in Figure 6, which displays the spectrum for the solvent, dimethyl sulfoxide (DMSO). The solvent signal is seen at 2.507 ppm, which is in excellent alignment with values reported in the literature. The signals collected strongly revealed that the water molecule was eliminated from the interaction between NH2 and CHO, which produces a CH=N group, and the anionic moiety with E-4B2HMP. It was confirmed by the downfield shift of the NH_2 signal from 2.64 ppm to 10.206 ppm. Due to the formation of the signal CH=N, which was shifted towards higher ppm, the signal NH2 in pure 2-(2-aminoethoxy) ethanol is at 2.64 ppm. Because of the electronegative character of bromine and intermolecular hydrogen bond, it interacts with adjacent protons, leading to the de-shielding of the hydrogen nucleus, which results in the pulling of electrons towards itself. After then, the resonance induced by the proton CH=N groups shifted to a higher ppm. The proton of phenol group signals was observed at 3.52 ppm in 2-(2-aminoethoxy) ethanol which was established by the signal 3.362 ppm in E-4B2HMP. However, the aromatic proton (Ar-H) because of powerful de-shielding due to the circulation of high electrons observed downfield at 10.9 – 8.5 ppm. A multiplet was observed between 7.63 ppm – 7.713 ppm, which corresponds to a hydrogen atom present in the aromatic ring. The doublet in 6.988 ppm and 6.971 ppm is due to the presence of primary alcohol in the compound. A singlet 10.991 ppm established the phenolic OH and intermolecular hydrogen bond in the new compound. A single 3.362 ppm has been attributed to the presence of the Br group in the compound E-4B2HMP.

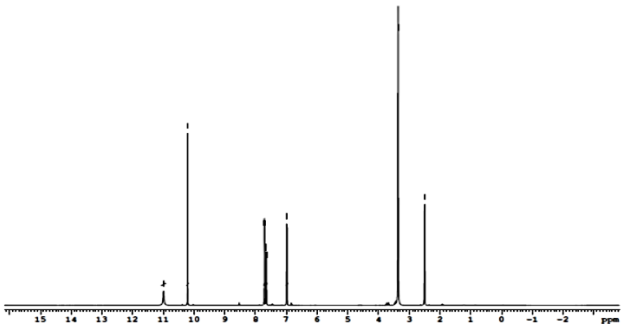

Figure 6. ^{1}H NMR spectrum of E-4B2HMP compound

Table 3. ^{1}H NMR and ^{13}C NMR chemical shift values in ppm of E-4B2HMP compound

NMR	Atom	E-4B2HMP chemical shift in ppm (δ)	Pure 5-Bromo-2-hydroxybenzaldehyde chemical shift in ppm (δ)	Pure 2-(2-aminoethoxy) ethanol chemical shift in ppm (δ)	Assignments
^{1}H	H1	10.206	9.84		C=N imine
	H2	10.91	10.92		OH
	H3, H4, H6	7.713, 7.707, 7.660	7.66		CH
	H5	6.97	6.91		C-Br
	H7	2.507		2.64	NH_2
	H8, H9, H10	7.65, 7.642, 7.637	7.62		CH
	H11	3.362		3.52	R-OH
^{13}C	C1	190.118	192.70		CHO
	C2	160.326	160.55		C-OH
	C5	111.176	111.34		C-Br
	C7	40.101, 40.268, 40.435		41.61,	C-NH_2
	C8	120.326	119.81		CH
	C9	138.892	139.63		CH
	C10	130.923	135.61		CH
	C11	124.443	121.77		C-C

3.4 FT-IR and FT-Raman spectra – Structure creation

Changes in the modes of vibration of molecules produce both Raman and FT-IR spectra. Thus, vibration modes are only Raman active when they change a molecule's dipole moment or polarizability, and they are only IR active when they do the same. The correlation between the symmetry of the molecule and its Raman and infrared activity can be explained by the law of mutual exclusion. However, this rule does not apply to molecules without a symmetry centre. Both Raman and FT-IR vibrations will be active in this scenario.

The E-4B2HMP compound's FT-IR and Raman spectra are shown in Figures 7 and 8. In FT-IR

study confirmed the functional groups in the region 4000 to 400 cm^{-1} (Mid-IR 2.5 – 25 µm). The mid-IR range of the E-4B2HMP compound is 6.8 µm to 22.1 µm. The 5-Bromo-2-hydroxybenzaldehyde's phenolic OH intermolecular hydrogen bond is responsible for the band observed at 3742.05 cm-1 in FT-IR. The vibrational stretch observed at 3041.45 cm^{-1} in the FT-IR and 3064.01 cm^{-1} in the FT-Raman spectrum are assigned to OH stretching vibrations of 2-(2-aminoethoxy) ethanol. The band at 2871.46 cm^{-1} in the FT-IR spectrum and the FT-Raman band observed at 2872.97 cm^{-1} are assigned to CH stretching vibration of 2-(2-aminoethoxy) ethanol. The band 3742.05 cm^{-1} in FT-IR is due to the intermolecular band of the new compound E-4B2HMP.

The imine group of CH=N stretching vibration involving coordination through the nitrogen of the azomethine-group is responsible for the vibration peak visible at 1651.21 cm-1 in FT-IR and FT-Raman bands recorded at 1670.09 cm-1 and 1662.64 cm-1, respectively. It attests to the creation of the novel chemical E-4B2HMP. The vibration peak at 1460.16 cm^{-1} in FT-IR and peak at 1464.87 cm^{-1} in FT-Raman assigned CH stretching. C-Br stretching is observed at 761.12 cm^{-1} in FT-IR and 765.05 cm^{-1} in FT-Raman. The band at 1265.03 cm^{-1} in FT-IR is due to the CH=N stretching of 2-(2-aminoethoxy) ethanol. The band at 884.04 cm^{-1} in FT-IR is due to the stretching of C-O of 2-(2-aminoethoxy) ethanol. The FT-IR and FT-Raman frequency assignments are summarized in Table 4.

Table 4. Absorption peaks in FT-IR and FT-Raman frequency assignments of E-4B2HMP compound.

Frequency in cm^{-1}		**Assignments**
FT-IR	**FT-RAMAN**	
3742.05	-	Phenolic OH Intermolecular hydrogen bond of 5-Bromo-2-hydroxybenzaldehyde
3041.45	3064.01	OH stretching of 2-(2-aminoethoxy) ethanol
2871.46	2878.97	CH stretching of 2-(2-aminoethoxy) ethanol
1651.21	1670.09, 1662.64	imine group C=N stretching of E-4B2HMP
1460.16	1464.87	CH stretching of 2-(2-aminoethoxy) ethanol
1265.03	1271.72	C-N stretching of 2-(2-aminoethoxy) ethanol
884.04	888.98	C-O stretching of 2-(2-aminoethoxy) ethanol
761.12	765.05	C-Br stretching of 5-Bromo-2-hydroxybenzaldehyde

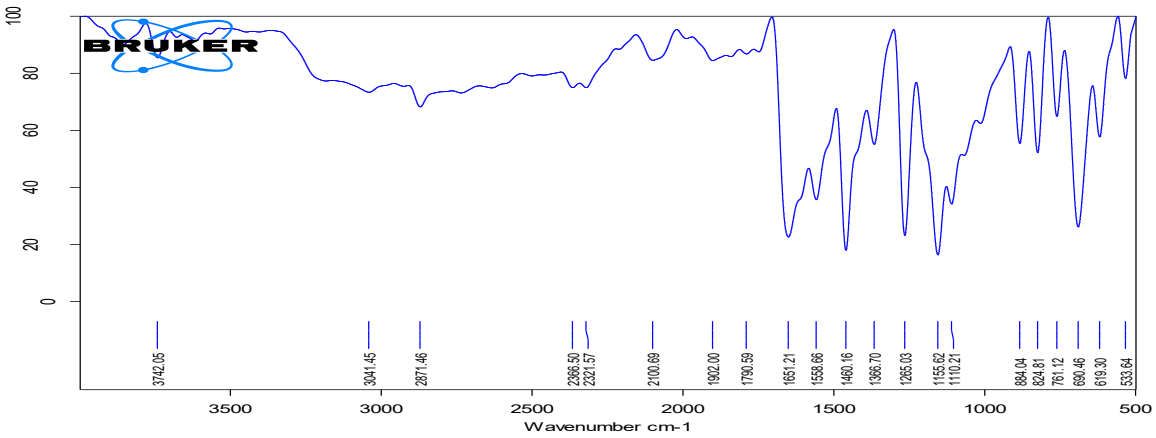

Figure 7. FTIR spectrum for E-4B2HMP compound.

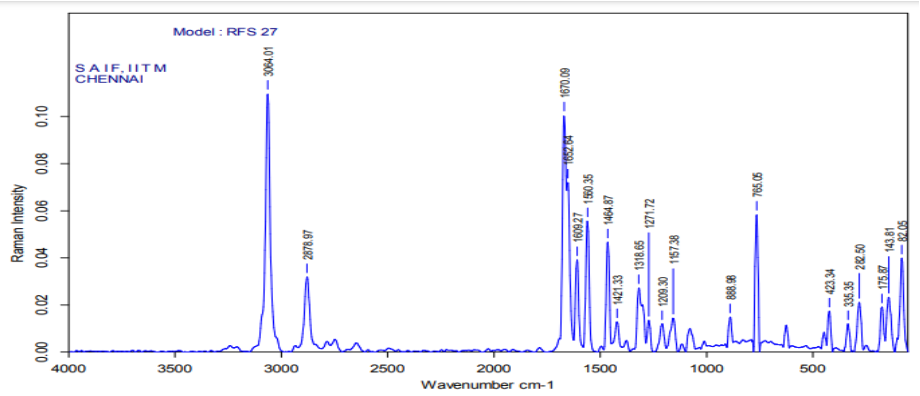

Figure 8. FT-Raman spectrum for E-4B2HMP compound.

3.5 Linear optical properties

The E-4B2HMP compound's UV-Vis spectra have been obtained between 200 and 400 nm. A UV-Vis spectroscopy data analysis proved the crystal's non-linear optical (NLO) feature, which has a band gap energy of 3.2 eV and a reduced cut-off wavelength of 387.5 nm. A broad band gap is a crucial beneficial effects for mid-IR nonlinear optical materials [4]. An attractive optical feature of the crystal is its large optical transmission window, which is crucial for non-linear optical (NLO) materials. Finding materials with high NLO, high transmittance, or low absorption in the near-infrared spectrum has become essential due to interest in optical applications such as switching [10]. Given its exceptional transparency over the visible spectrum, the crystal may be appropriate for NLO application for bioimaging. [12]. The absorbance spectra of invented E-4B2HMP crystals are shown in Figure 9.

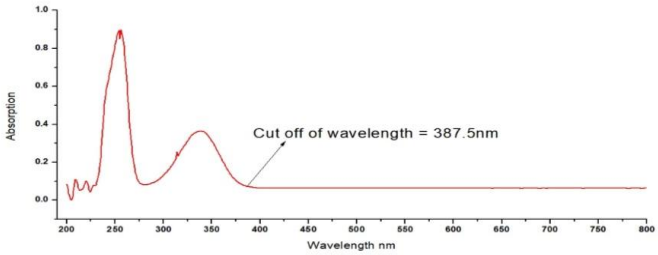

Figure 9. UV-vis absorption spectrum of E-4B2HMP compound

3.5.1 Refractive index

The Refractive index is the ultimate property of an optical material. Reflectance (R) and refractive index of the crystal in terms of transmittance are expressed as (Swanepoel method 1983),

$$n = [N + (N - S^2)^{1/2}]^{1/2}$$

Where,

$$N = 2S \frac{Tmax - Tmin}{TmaxTmin} + \frac{S^2+1}{2},$$

Where T_{max} and T_{min}, are the transmittance max and the correlating minimum at that wavelength (λ). It used a well-recognized part of the mathematical equation.

$$S = \frac{1}{Ts} + \left(\frac{1}{Ts} - 1\right)^{1/2}$$

The refractive index was calculated as n = 1.4 of E-4B2HMP at 387.5 nm, suggesting that the material will enhance the performance of optical properties [13]. Figure 10 shows the

refractive index with the wavelength of the E-4B2HMP crystal. The refractive index decreases as wavelength increases. The higher band gap transmission in the overall region and lower refractive index make the crystal suitable for good pharmaceutical applications [14].

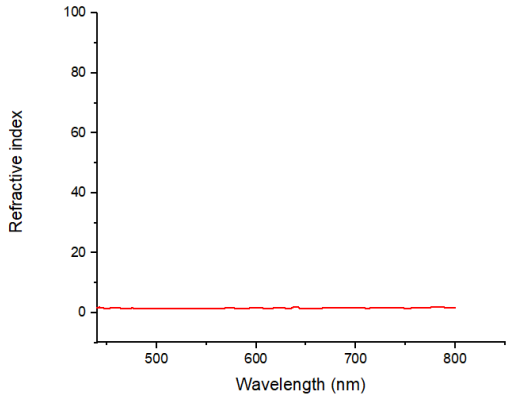

Figure 10. The refractive index of the E-4B2HMP compound

3.6 Photoluminescence

Photoluminescence (PL) spectroscopy is one of the practical tools to provide direct information about the physical properties of materials at the molecular level, including shallow and deep level defects and band gap states [15]. Figure 11 displays the photoluminescence (PL) distribution of the E-4B2HMP crystal, which is recorded between 350 and 600 nm. The crystal's green emission is apparent in the high-intensity fluorescence spectrum at 521.7 nm. The intensity and broadness of the peak reveal the crystalline nature. The band-gap energy of the E-4B2HMP crystal has been calculated to be 2.4 eV, using the formula $E_g = 1.24/\lambda$ eV. Where λ is the fluorescence wavelength [11].

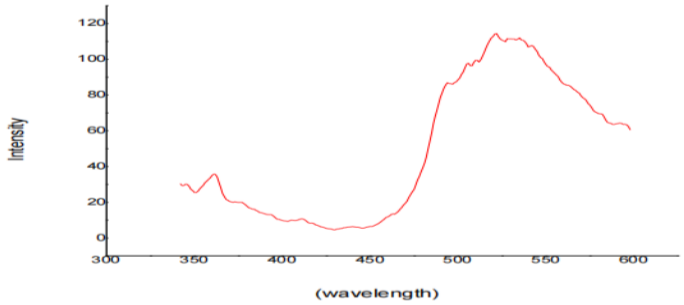

Figure 11. Photoluminescence spectrum of E-4B2HMP compound

3.7 Laser damage threshold studies

The Laser Damage Threshold (LDT) of E-4B2HMP crystal has been measured using Nd: YAG laser. For the E-4B2HMP crystal, the biconvex lens has an energy level of 76.3 mJ, a length of focus 10 cm, and a pulse width of 6 ns at 1064 nm with a repetition rate of 10 Hz. Using a power meter that destroys crystals, the energy density of the laser beam was measured. The E-4B2HMP crystal's threshold for laser

damage is 40.4989 MW/cm^2, and it is calculated from the relation [11],

$$\text{Power density P(d)} = \frac{E}{\tau\pi r^2}.$$

Where E is the input energy (mJ), τ is the pulse width (ns), and r is the radius of the circular spot size (cm^2). The measured multiple-shot laser damage threshold values are 40.4989 MW/cm^2, higher than the KDP. The surface damage of the crystal using a high-power laser limits the performance of the NLO pharmaceutical applications of the materials [15].

3.8 Z-scan Measurements

A simple to understand highly precise method for figuring out the nonlinear absorption coefficient β and the nonlinear index of refraction n2 is the Z-scan technique [16]. This nonlinear index of refraction is proportional to the third-order susceptibility's real part. (Reχ(3)) Furthermore, [Imχ(3)] is proportional to the nonlinear absorption coefficient. A 532 nm diode pumped solid state laser focussed by a 103 mm focal length lens was used for the Z-scan tests. It was determined that the focal point's intensity (I∘) and beam waist (ω∘) were 0.0136 MWcm-2 and 0.33 μm, respectively. Since the experimental setup's Rayleigh range (Z∘ = πω∘/ λ) was determined to be 1.32 mm, the thin sample approximation criterion L < z∘ was satisfied.

The schematic of the experimental set up used is shown in Figure 12.

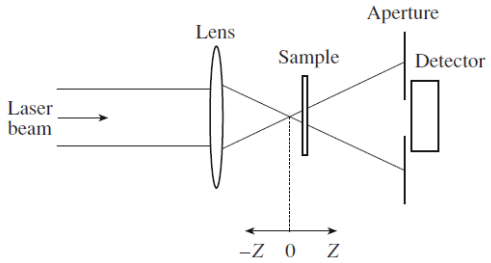

Figure 12. Schematic of experimental setup for z-scan

The focal region is translated along the axial direction, which is the direction of the propagation laser beam, by a 1 mm wide optical cell that contains the E-4B2HMP sample in acetic acid solvent. Using a Si photodiode detector that was fed into a dual channel detector measurement unit, the beam's transmission through an aperture in the far field was measured. In an open aperture Z-scan, the aperture was swapped out for a lens that would gather the full laser beam that was sent through the sample.

Figure 13(a) and Figure 13(b) show the closed-to-open normalized Z-scan of the E-4B2HMP sample in acetic acid solvent at 62% transmittance in both closed and open modes. A valley-normalized transmittance derived from the closed aperture Z-scan data shows a peak after which the refraction nonlinearity has a negative sign, meaning it is self-defocusing. Local temperature variations in the refractive index are the cause of the self-defocusing effect. The transmission minimum at focus in the open aperture Z-scan pattern indicated reverse saturable absorption (RSA)

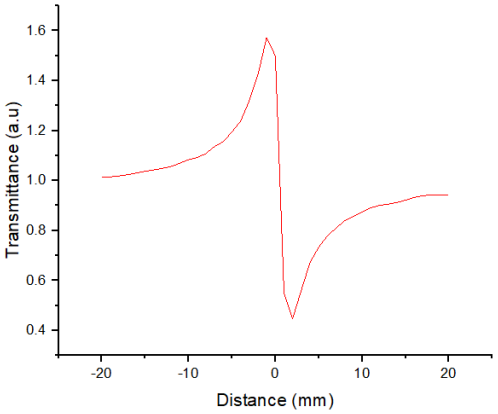

Figure 13(a) Closed aperture

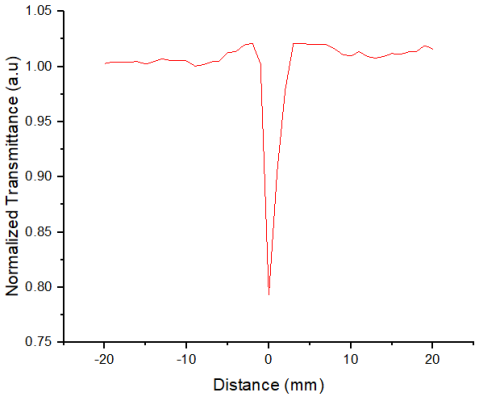

Figure 13 (b) Open aperture

The difference of the normalized peak and valley transmittances, Tp/Tv, is the measurable quantity Tp-v. This quantity's change as a function of |Δϕo| is provided by

$$\Delta T_{p-v} = 0.406(1-S)^{0.25}\left|\Delta\phi_o\right| \quad (1)$$

where $\Delta\phi_0$ is the on-axis phase shift at the focus. S the aperture linear transmittance is given by

$$S = 1 - \exp(-2\, r_a^2/\omega^2) \quad (2)$$

with r_a denoting the aperture radius and ω_a denoting the radius of the laser spot before the aperture.

The on-axis phase shift is related to the third order nonlinear refractive index (n_2) [17] by,

$$|\Delta\phi_0| = k n_2 L_{eff} I_0 \quad (3)$$

where $L_{eff} = (1-e^{-\alpha L})/\alpha$, with L the sample length, α is the linear absorption coefficient I_O is the intensity of the laser beam at focus z = 0, and k is the wave number (k=2π/λ)

The third-order nonlinear optical susceptibility's imaginary portions are computed using the following relations and the nonlinear absorption coefficient β value derived from the open aperture Z-scan data:

$$q_o(z) = \frac{\beta . I_o . L_{eff}}{(1+\frac{Z^2}{Z_o^2})} \quad (4)$$

$$\beta = \frac{2\sqrt{2}.\Delta T}{I_o . L_{eff}} \quad (5)$$

$Z_R = k\omega_0^2/2$ is the diffraction length of the beam, ω_0 is the beam waist radius at the focal point.

Experimentally determined nonlinear refractive index n_2 and nonlinear absorption coefficient β can be used in finding the real and imaginary parts of the third-order nonlinear optical susceptibility [χ^3] [18] according to the following relations.

$$\mathrm{Re}\,\chi^3(esu) = 10^{-4}\frac{\varepsilon_o c^2 n_o^2}{\pi} n_2 (\frac{cm^2}{W}) \quad (6)$$

$$I_m\chi^3(esu) = 10^{-2}\frac{\varepsilon_o c^2 n_o^2 \lambda}{4\pi^2}\beta(\frac{cm}{W}) \quad (7)$$

where ε_0 is the vacuum permittivity, and c is the light velocity in vacuum.

The absolute value of the third-order nonlinear optical susceptibility is given by the relation

$$|\chi^3| = [(R_e(\chi^3))^2 + (I_m(\chi^3))^2]^{1/2} \quad (8)$$

The nonlinear parameters calculated are as tabulated in Table 5

Table 5. Nonlinear parameters of E4B2HMP

$n_2 \times 10^{-9}$ cm²/W	$\beta \times 10^{-4}$ cm/W	Re $\chi^{(3)} \times 10^{-6}$ esu	Im $\chi^{(3)} \times 10^{-6}$ esu	$\chi^{(3)} \times 10^{-6}$ esu
4.230x10^{-9} cm²/W	0.00123x10^{-4} cm/W	0.00000479 x10^{-6} esu	9.446082 x10^{-6} esu	4.887 x10^{-6} esu

3.9 In-silico ADME analysis

The initial stage of drug development involves identifying acceptable candidates with drug-like properties and enough knowledge of absorption, distribution, metabolism, and excretion (ADME). Physicochemical characteristics, pharmacokinetics, solubility, lipophilicity, drug-likeness determined by violation of Lipinski's rule of five, and medicinal chemistry were among the ADME descriptors examined utilising the SwissADME online server [19]. These results are tabulated in Table 6.

Table 6. ADME Analysis of E-4B2HMP Crystal Structure

S. No	Descriptors	E-4B2HMP compound
Physicochemical Properties		
1.	SMILE	Oc1ccc(cc1C=NCCOCCO)Br
2.	Formula	$C_{11}H_{14}BrNO_3$
3.	Molecular Weight	288.14 g/mol
4.	Number of heavy atoms	16
5.	Number of aromatic heavy atoms	6
6.	Fraction Csp3	0.36
7.	Number of rotatable bonds	6
8.	Number of H-bond acceptors	4
9.	Number of H-bond donors	2
10.	Molar refractivity	66.29
11.	Topological polar surface area	62.05Å^2
Lipophilicity		

12.	Log $P_{o/w}$ (iLOGP)	2.50
13.	Log $P_{o/w}$ (XLOGP3)	1.00
14.	Log $P_{o/w}$ (WLOGP)	1.58
15.	Log $P_{o/w}$ (MLOGP)	0.99
16.	Log $P_{o/w}$ (SILICOS-IT)	2.85
17.	Consensus Log $P_{o/w}$	1.78
Water Solubility		
18.	Log S (ESOL) Solubility Class	-2.14 2.10e+00 mg/ml; 7.28e-03 mol/l Soluble
19.	Log S(Ali) Solubility Class	-1.89 3.70e+00 mg/ml; 1.28e-02 mol/l Very Soluble
20.	Log S (SILICOS-IT) Solubility Class	-3.55 8.18e-02 mg/ml ; 2.84e-04 mol/l Soluble
Pharmacokinetics		
21.	GI absorption	High
22.	BBB permeant	Yes
23.	P-gp substrate	No
24.	CYP1A2 inhibitor	Yes
25.	CYP2C19 inhibitor	No
26.	CYP2C9 inhibitor	No
27.	CYP2D6 inhibitor	No
28.	CYP3A4 inhibitor	No

29.	Log Kp (skin permeation)	-7.35 cm/s
Druglikeness		
30.	Lipinski	Yes; 0 violation
31.	Ghose	Yes
32.	Veber	Yes
33.	Egan	Yes
34.	Muegge	Yes
35.	Bioavailability Score	0.55
Medicinal Chemistry		
36.	PAINS	0 alert
37.	Brenk	1 alert: imine_1
38.	Leadlikeness	Yes
39.	Synthetic accessibility	2.77

3.10 In-vitro evaluation of Anti-cancer Activity

The anticancer activities of E-4B2HMP crystal were tested on human lung cancer cell line(A549). The cancer cell growth inhibition activity of newly synthesized compound E-4B2HMP was assessed invitro on human cancer cell (A549) after a continuous exposure for 48h. The compound was dissolved in DMSO at 1µm. The E-4B2HMP showed higher toxicity at 100 µM and lowest at 10µM concentration in A549 cell line. A549 are ~5µM, ~25µM, ~50µM, ~75µM and ~100µM results were shown in Figure 14.

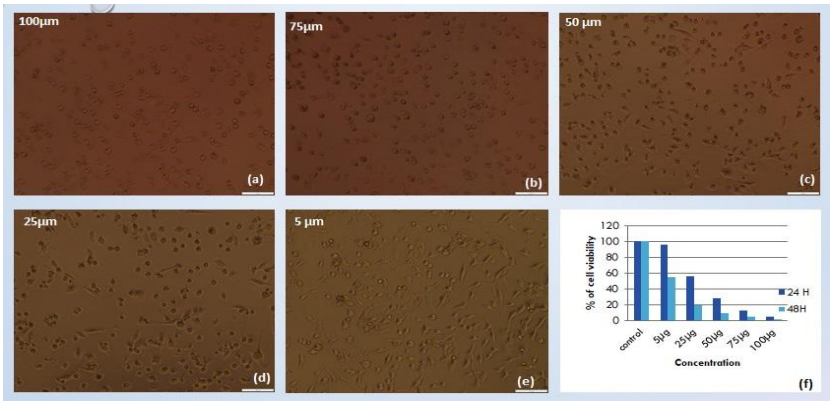

Figure 14. Anti-cancer Activity of E-4B2HMP

3.11 Molecular Docking

A method known as docking predicts the preferred conformation and binding of a small ligand and a big protein molecule. Protein Data Bank (PDB) was mined for the chosen EGFR(PDB ID: 2j6m) targeting the protein in Cancer cell. The docking score is -5.3 Kcal/mol. Docking against the EGFR is shown in Figure 15 (a), and 2D interaction is displayed in Figure 15 (b).

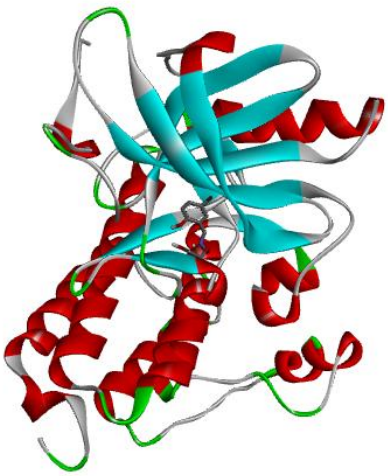

Figure 15(a). The molecular docking result of the E-4B2HMP with EGFR protein

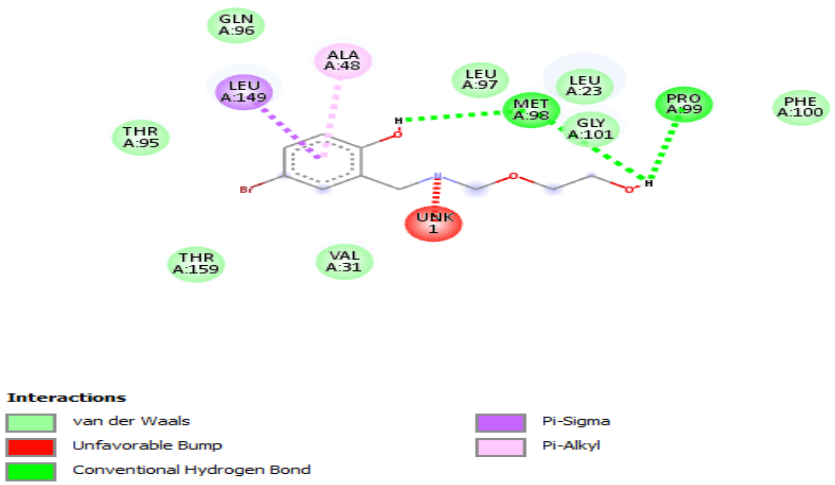

Figure15 (b) 2D interactions

Conclusion

The New Crystal is identified in the amine family and its structure was solved and deposited in CCDC. The structural Property Relationship approach found the relationships between chemical structure and related structural properties including the target property of the studied crystal (Bio-imaging) for in-vitro bio-imaging applications and being ideal for lung cancer disease diagnosis. The linear refractive index is calculated from the Swanepoel method and the nonlinear refractive index is calculated from the Z-scan method. It is concluded that Schiff-based molecular crystal contains recognizable molecules within the structure and is held together with intermolecular hydrogen-bonding by the result obtained. In Photoluminescence spectroscopy NLO property of the Schiff-based crystal was well investigated through green emissions. The generated E-4B2HMP crystal will be the potential candidate in bio-imaging which was investigated by the multi-emission peak in Photoluminescence Spectroscopy.

Electronic supplementary Information

CCDC 2224027 contains supplementary Crystallographic Data of E-4B2HMP, that can be obtained freely from the Cambridge crystallographic data center via www.ccdc.cam.ac.uk/data_request/cif.

Credit authorship contribution Statement

The idea and design of the study were contributed to by all authors. preparation of materials, gathering of data, conceptualization, methodology, software, and writing—creation of the first draft by **J. Priyanka.,** Supervision, Reviewing and Editing, Project Administration by **R. Ida Malarselvi,** Resources by **G. Vinitha,** Validation by **C. Ramachandra Raja,** Visualization by **R. Priscilla** and all authors commented on previous versions of the manuscript. The final manuscript was read and approved by all authors.

Data availability

No data was used for the research described in the article.

Funding

No particular funding from public, private, or nonprofit organizations was given to this research.

Acknowledgments

As part of this work, SCXRD, and NMR Spectroscopy characterization techniques were conducted in Sophisticated Analytical Instruments Facility (SAIF), Indian Institute of Technology, Madras, Chennai – 600 036, Tamil Nadu, India. UV-Vis-NIR spectroscopy characterization technique was conducted at Sathyabama University, Chennai, Tamil Nadu, India. PXRD and Photoluminescence characterization was conducted at the University Science Instrumentation Centre (USIC), Alagappa University, Karaikudi - 630 003, Tamil Nadu, India. Also, the authors place on record special thanks to Dr. G. Vinitha, For giving them a third-order nonlinear testing facility to record Z-scan measurements, thanks to VIT, Chennai.

Reference:

[1] Wei Huang, Zhiyu He, Beijun Zhao, Shifu Zhu, Baojun Chen, "Crystal growth, Structure and optical properties of new quaternary chalcogenide nonlinear optical crystal $AgGaGeS_4$", Journal of Alloys and compounds, Elsevier, 2019, https://doi.org/10.1016/j.jallcom.2019.05.066

[2] V. Sriraman, E. Vinoth, M. Nizam Mohideen, P. K. M. Imran, A. Arun, "Synthesis, Crystal structure, DFT, docking and biological activity studies of (NZ-N'Z)-3,3'-(piperazine-1,4-diyl) bis (N-(-4-methyl benzylidene) propane -1-amine)", Materials Chemistry and Physics, Elsevier, 2022, https://doi.org/10.1016/j.matchemphys.2021.125220

[3] M. D. Aggarwal, J. Choi, W. S. Wang, K. Baht, R. B. Lal, Angela D Shields, Benjamin G Penn, Donald O Frazier, "Solution growth of a novel nonlinear Optical material: L-histidine tetrafluoroborate", Journal of Crystal Growth, Elsevier, 1999, https://doi.org/10.1016/S0022-0248(99)00200-6

[4] Weimin Dong, Qian Yao, Junying Zhang, Lintao Liu, Jing Li, and Jiyang Wang, "Czochralski Growth and Characterization of a Novel Nonlinear Optical Crystal Te2P2O9", Crystal Growth & Design, ACS Publications, 2018, https://doi.org/10.1021/acs.cgd.8b00680

[5] P. Karuppasamy, T. Kamalesh, K. Anitha, S. Abdul Kalam, Muthu Senthil Pandian, P. Ramasamy, Sunil Verma, S. Venugopal Rao, "Synthesis, Crystal growth, Structure and Characterization of a novel third order nonlinear optical organic single crystal: 2-Amino 4, 6-Diethyl Pyrimidine 4-nitrophenol", Optical materials Elsevier, 2018, doi:10.1016/j.optmat.2018.07.039

[6] P. Vijayakumar, G. Anandha Babu, P. Ramasamy, "Synthesis, crystal growth and characterization of nonlinear optical organic crystal: P-Toluidinium P-Toluenesulphonate", Materials research bulletin, Elsevier, 2012, https://doi.org/10.1016/j.materresbull.2012.01.011

[7] B. Sahaya Infant Lasalle, Muthu Senthil Pandian, K. Anitha, P. Ramasamy, "Crystal growth and characterization of piperazinium mercuric chloride (PMC) single crystal for nonlinear optical (NLO) application", Inorganic Chemistry Communications, Elsevier, 2023, https://doi.org/10.1016/j.inoche.2023.111397

[8] Colan E. Hughes, G. N. Manjunatha Reddy, Stefano Masiero, Steven P. Brown, P. Andrew Williams, Kenneth D. M. Harris, "Determination of a Complex Crystal Structure in the Absence of Single Crystals: Analysis of Powder X-ray Diffraction Data, Guided by Solid-State NMR and Periodic DFT Calculations, Reveals A New 2'-Deoxyguanosine Structural Motif", Chemical Science, RSC Publications, 2017, https://doi.org/10.1039/c7sc00587c

[9] Jurgen Bruning and Martin U. Schmidt, "The determination of crystal structures of active pharmaceutical ingredients from X-ray powder diffraction data: a brief, practical introduction, with fexofenadine hydrochloride as example", Journal of Pharmacy and Pharmacology, 2014, https://doi.org/10.1111/jphp.12374

[10] William I.F .David ,Kenneth shankland,jacco van de streek, elna pidcock, W.D.samuel motherwell and Jason C.cole, "DASH: a program for crystal structure determination from powder diffraction data", Journal of Applied crystallography,2006, https://doi.org/10.1107/S0021889806042117

[11] D. Bharath, S. Kalainathan, "Synthesis, growth, thermal and optical studies on third order nonlinear optical material (E)-2-{3-[2-(4-chlorophenyl) vinyl]-5,5-dimethylcyclo-hex-2-en-1-yildene} malononitrile for opto-elctronic application", Spectrochimica Acta Part A: Molecular and Biomolecular Spectroscopy, Elsevier, 2014, https://doi.org/10.1016/j.saa.2013.10.001

[12] S. Rafi Ahamed, J. Balaji & P. Srinivasan, "Growth and Characterization of Organometallic NLO material: cesium hcontriydrogen tartrate", Material Research Innovations, Taylor & Francis, 1432-8917, 2017, https://doi.org/10.1080/14328917.2017.1320837

[13] R. Ida Malarselvi, G. Swetha, C. Ramachandra Raja, R. Pricilla, "An analysis of thermal decomposition of (E)

– 4- Iodo – 2 – [(Phenylimino)Methyl] Phenol crystal compared to Thermogravimetry (TG), and Fourier transform infrared (FTIR) techniques", International Journal of Pharmaceutical Research, 2020, https://openurl.ebsco.com/EPDB%3Agcd%3A7%3A30208215/detailv2?sid=ebsco%3Aplink%3Ascholar&id=ebsco%3Agcd%3A155797356&crl=f&link_origin=www.google.com

[14] Hiral Raval, B. B. Parekh, K. D. Parikh and M. J. Joshi, "Growth and Characterizations of Organic NLO Imidazolium L-Tartrate (IMLT) Single Crystal", Advances in Condensed Matter Physics, 2019, https://doi.org/10.1155/2019/3853215

[15] M. Divya Bharathi, G. Ahila, J. Mohana, R. Bhuvaneswari, G. Anbalagan, "Crystal growth and optical characterization of an organic single crystal for frequency conversion applications", IOP Conference Series: Materials science and Engineering, 2018, https://iopscience.iop.org/article/10.1088/1757-899X/360/1/012057

[16] Sheik-Bahae, M., Said, A.A., Wei, T., Hagan, D.J., and Van Stryland, E.W.: 'Sensitive measurement of optical nonlinearities using a single beam', IEEE J. Quantum Electron., 1990, QE-26, pp 760-769, https://ieeexplore.ieee.org/document/53394

[17] T.D. Krauss, F.W. Wise, Appl. Phys. Lett. 65 (1994) 1739.

[18] Vinitha G. and Ramalingam A., 'Nonlinear Studies of Acid Fuchsin dye in liquid and solid media', Spectrochimica acta part A: Molecular and Biomolecular Spectroscopy, 69 (2008) pp.1160–1164, https://doi.org/10.1016/j.saa.2007.06.016

[19] Soniya Sharma, Fateme Salehi, Bernd W. Scheithauer, Fabio Rotondo, Luis V. Syro and Kalman Kovacs, "Role of MGMT in Tumor Development, Progression, Diagnosis, Treatment and Prognosis", Anticancer Research, 2009, https://ar.iiarjournals.org/content/29/10/3759